NASA TN D-1621

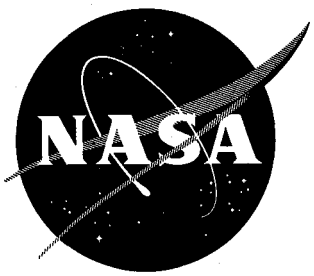

TECHNICAL NOTE

D-1621

A 6-INCH SUBSONIC HIGH-TEMPERATURE ARC TUNNEL FOR STRUCTURES AND MATERIAL TESTS

By Ronald D. Brown and L. Ross Levin

Langley Research Center
Langley Station, Hampton, Va.

NATIONAL AERONAUTICS AND SPACE ADMINISTRATION
WASHINGTON
April 1963

NATIONAL AERONAUTICS AND SPACE ADMINISTRATION

TECHNICAL NOTE D-1621

A 6-INCH SUBSONIC HIGH-TEMPERATURE ARC TUNNEL FOR STRUCTURES AND MATERIAL TESTS

By Ronald D. Brown and L. Ross Levin

SUMMARY

A 6-inch subsonic arc tunnel utilizing three-phase a-c water-cooled copper electrodes has been developed at the Langley Research Center to evaluate the performance of ablation materials under simulated reentry conditions. The tunnel is capable of producing a range of stagnation pressures from 0.16 to 1.0 atmosphere and stagnation temperatures up to 4400° K for periods of time up to 90 seconds limited by air storage capacity. Heat-transfer rates up to 70 Btu/ft^2-sec can be obtained on a 3-inch-diameter flat-face body in the 6-inch-diameter stream. Ablation materials can be evaluated in the stream at stagnation enthalpies up to 4,000 Btu/lb. Three commercially available materials, Teflon, nylon, and Fluorogreen, were tested as ablation materials in the 6-inch subsonic arc tunnel at the Langley Research Center, and the results are in reasonable agreement with theoretical predictions and previously published experimental data.

INTRODUCTION

The leading edges and stagnation points on vehicles reentering the earth's atmosphere encounter severe aerodynamic heating. The reentry of a hypersonic-glider-type vehicle may take one-half hour or more, and the period of most severe heating may last several minutes. A blunt body at reentry velocities generates a normal shock so that the air flow in the vicinity of the stagnation point on the body is subsonic and at a very high temperature. The range of stagnation air temperatures accompanying the most severe heating is from 5000° K to 8000° K depending upon the trajectory of the vehicle. This temperature is well above any temperature that has been obtained for a sufficient time duration from a chemical-reaction or conventional heat-exchanger type of facility. However, a high-intensity electric arc can heat air to temperatures above 6000° K. Proper design of electrodes and arc chamber will produce a high-temperature air stream for a sufficient length of time to permit materials and structures tests.

In a high-temperature subsonic tunnel, the stagnation temperature, stagnation pressure, and stagnation-point heat-transfer rate can match those at a particular altitude and velocity condition. Within the range of stagnation pressure and temperature of a particular subsonic facility, the stagnation-point heat-transfer rate can be simulated by adjusting model scale.

A 6-inch subsonic arc tunnel that utilizes a three-phase a-c water-cooled copper electrode arc to heat the air in the settling chamber was constructed at the Langley Research Center to perform materials tests at simulated reentry conditions. This report will describe this facility, present the calibration values and operating range, and describe ablation tests that were performed to determine applicability of this facility to evaluate basic ablation material properties. A discussion of the ablation calculations is included in the appendix.

SYMBOLS

A	area
C_p	specific heat at constant pressure
h	enthalpy
h_{eff}	effective heat of ablation
H	heat that the body absorbs at zero enthalpy potential (eq. (A7))
h_m	latent heat of melting
h_v	latent heat of vaporization
K	slope of curve for variation of heat of ablation with boundary-layer enthalpy potential (eq. (A8))
l	ablation material thickness
$\dot{m}$	mass loss per unit area per unit time
M	Mach number
N_{Pr}	Prandtl number
p	pressure
$\dot{q}$	heat-transfer rate
R	body radius
t	time
T	temperature
$\dot{w}$	tunnel flow rate
u	velocity

x	surface distance from stagnation point
Z	compressibility factor
ρ	density
τ	thickness

Subscripts:

b	body
e	edge of boundary layer
f	final
i	initial
o	hot body
s	stagnation
w	wall
∞	free stream
1	foreign gas
2	air

DESCRIPTION OF 6-INCH SUBSONIC ARC TUNNEL

The arc tunnel is essentially a subsonic wind tunnel with a 6-inch axisymmetric test section that is supplied with air heated up to 4400° K by an a-c arc unit. The arc unit utilizes a three-phase water-cooled copper electrode configuration that is supplied by an a-c power system of 3,300 kilovolt amperes, 600 volts phase to ground. A photograph and a schematic diagram of the tunnel are shown in figures 1 and 2. The primary air or test medium is regulated from a compressed-air storage supply. An auxiliary air-operated ejector is used to permit operation of the tunnel with a test-section pressure less than atmospheric.

The principal parts of the arc tunnel are described in subsequent paragraphs.

Arc Unit

The arc unit consists of the electrode configuration and an arc chamber. The water-cooled copper electrode configuration is shown in the photograph in figure 3. There are three pairs of electrodes, each pair consisting of two concentric water-cooled copper rings. Each 3-inch-diameter center electrode is

connected to one phase of the three-phase a-c power supply. The 6-inch-diameter outside electrodes have a common connection to the grounded neutral of the electrical power supply. The electrode pairs are equally spaced. The grounded electrode rings are mounted on a steel plate that is 1 inch thick. The inner rings of each pair pass through the steel plate and are electrically insulated from the plate by bushings. A schematic diagram of the electrical power system and the system for measuring the arc current, voltage, and power is shown in figure 4.

The steel plate or head is mounted onto the arc chamber that has an 18-inch inside diameter. The arc chamber is a double-walled vessel, water cooled, and lined with a graphite sleeve. The tunnel air is sprayed into the arc chamber from a plenum chamber in the foamed-quartz plate that is used to protect the steel plate from the radiation of the arcs. A graphite baffle plate encloses the grounded outside electrodes so that the air must pass through the arcing area. An electromagnetic field coil surrounds the arc chamber in the same plane as the electrodes and is used to produce a magnetic flux along the axis of the arc unit. The coil is energized by a direct-current source.

The arc is initiated by shorting a pair of electrodes with a small copper wire. When the electrical circuit is closed, the current causes the copper wire to vaporize. This copper vapor provides enough ionized particles that the arc can be established and maintained between the electrodes.

The axial magnetic field through the arc unit rotates the arc at two to three revolutions per one-half cycle. The arc changes direction each half-cycle because the electrode current changes direction, while the direction of the magnetic field is the same at all times. The rotation of the arc minimizes localized heating of the electrodes. The arc rotation along with effective water cooling permits an average electrode life of 60 minutes total when running at currents of 3,500 amperes. The electrode cooling requires a water-flow rate of 15 gallons per minute at an input pressure of 200 pounds per square inch gage for each electrode. This flow, at maximum arc power, results in a maximum water temperature rise of 80°. The electrode material that is vaporized results in a contamination of approximately 0.05 percent by weight.

Subsonic Tunnel and Ejector

The arc unit (see fig. 2) is in effect the settling chamber of the subsonic wind tunnel. The area contraction ratio from the arc plane to the 6-inch-diameter test section is 7.1 and the distance from the arc plane to the test section is 4 test-section diameters. The subsonic axisymmetric nozzle discharges into a 6-inch-diameter graphite liner that lines the 8-inch straight section of the tunnel up to test-section windows. The test section was constructed from solid steel and is open in the sense that the model is tested in a 6-inch-diameter stream in an 8-inch physical diameter. Six-inch-diameter windows are mounted on tubes on both sides of the test section. An auxiliary air-operated ejector was used to permit operation at test-section pressures less than atmospheric. The ejector was designed with information from reference 1. Reference 2 gives some pumping characteristics of a similar ejector. The maximum operation time of the ejector and consequently the tunnel is limited to approximately 90 seconds because of the limitation of the air storage capacity.

The static pressure in the test section can be regulated by adjusting the minimum area at the ejector with the "plug" shown in figure 2. The minimum area, being the sonic point, is decreased when the "plug" diameter is increased. Therefore, for a given tunnel air-flow rate and stream temperature the test-section pressure increased with increased diameter plug.

Model Insertion Mechanism

The model is mounted on a sting and door arrangement that is located in a sealed box below the test section. The model is protected from the stream during the starting portion of the run by a door. When the tunnel is at the desired operating conditions, the protection door is removed by a pneumatically operated piston and the door with the attached model is inserted. The model moves from the edge of the stream to within 1/4 inch of the center of the stream in approximately 0.03 of a second. An additional 0.13 second is required for the model to move the final 1/4 inch to the center of the stream because of the cushion effect at the end of the piston travel. This "cushion" effect makes the total time from edge to center of the stream about 0.16 of a second. The model can be tested for a given time by setting the desired insertion and removal times on a sequencer.

MEASUREMENT OF TUNNEL CONDITIONS

Tunnel Air-Flow Rate

The air to be heated was supplied either from a high-pressure storage tank or by induced flow from the atmosphere. When the air was obtained from the storage tank, the flow was regulated by a throttling valve and measured by an orifice meter downstream of the valve. The induced flow from the atmosphere was used on several tests when the arc chamber was less than atmospheric. The induced flow was measured with a Laval flow meter and regulated by an orifice downstream of the meter.

Free-Stream Pressure

The static pressure in the test section was measured by using strain-gage pressure transducers and was recorded continuously on an oscillograph. A 0.050-inch-diameter stainless-steel tube was used to connect the pressure gage to the free-stream pressure orifice so that the gage would not be in direct contact with the high-temperature gas.

Free-Stream Temperature

The free-stream temperature at the test section was measured spectrographically by an atomic line intensity ratio method using the electronic excitation spectrum of copper that appears in the gas caused by the small contamination from electrodes. This temperature measurement system is discussed in detail in reference 3. A simple medium glass spectrograph, with a 60° prism and an

f-number 11.7, was used in conjunction with a photoelectric readout system for recording the intensity ratio of the copper lines at 5153 A and 5700 A. The temperature of the tunnel air, thermodynamic equilibrium being assumed, is a function of this intensity ratio. The free-stream temperature was measured 1 inch forward of the stagnation point of the model in each test.

Velocity Calculation

The average velocity in the test section can be calculated from the pressure and temperature measurements by using the continuity equation.

$$u_\infty = \frac{\dot{w}}{\rho_\infty A}$$

The density can be obtained from reference 4 as a function of temperature and pressure.

MODELS AND MATERIALS

Water-Cooled Heat-Transfer Probe

The heat-transfer rate was measured with a 3/8-inch-diameter water-cooled continuous-recording calorimeter mounted in the test section above the model with its axis parallel to the center line. This calorimeter, which is shown in figure 5, gives a continuous recording of the heat-transfer rate during a test. A copper wire is attached to the center of constantan foil disk which is soldered around its perimeter to a water-cooled copper plug. A heat flux on the face of the calorimeter generates a heat flow radially from the center of the constantan disk to the cooled copper plug and generates a millivolt output. The millivolt output is measured in the circuit formed by the copper wire, the constantan foil, and the copper plug. The hot junction is the wire-to-foil connection and the cold junction is the foil-to-copper plug connection. The information necessary to determine the sensitivity and time constant for this type of calorimeter is given in reference 5. The cooling water flow was 0.33 gallon per minute at an input pressure of 200 pounds per square inch gage.

3-Inch-Diameter Heat-Transfer-Distribution Model

A 3-inch-diameter flat-face Inconel model with a corner-to-body-radius ratio of 0.0834, shown in figure 6(a), was used for the determination of stagnation-point heat-transfer rate for the different running conditions. Thermocouples were located along the back surface of the model as shown in the figure. The actual thickness of material at each thermocouple location was measured.

Ablation Specimens

The ablation specimens were of the same shape as the 3-inch flat-face heat-transfer model. The ablation material was mounted on a support body by the screws that are shown with other details of the ablation specimen in figure 6(b). The ablation materials tested to determine the usefulness of this facility were commercially available Teflon, nylon, and Fluorogreen.

TEST PROCEDURE

Calibration

A preliminary test was conducted to determine the range of free-stream temperature that could be obtained at one power setting. The 3/8-inch-diameter continuous-recording heat-transfer-rate probe was placed in the test section 2 inches from the center of the 6-inch-diameter stream. The arc chamber and test section were pumped down to the desired starting pressure (less than atmospheric) by using the auxiliary air-operated ejector and the arc unit was started. The tunnel air-flow rate was held constant for 10 seconds in order to obtain a heat-transfer-rate indication on the probe and a free-stream temperature measurement. After the heat-transfer-rate indication and temperature were obtained, the tunnel air-flow rate was changed to another value and the process was repeated. Sufficient readings were taken so that three flow settings could be selected that would give a large enthalpy range.

The 3-inch-diameter flat-face Inconel heat-transfer-distribution model was mounted in the tunnel standby chamber so that, when injected into the stream, it would be in the same plane as the continuous-recording heat-transfer probe. From the upper side of the heat-transfer model to the lower side of the 3/8-inch probe was only 5/16 of an inch. The tunnel was started and brought up to the desired air-flow rate. The heat-transfer model was then injected into the flow and removed in about 0.6 of a second. This procedure was repeated several times for each air-flow rate. Thus a calibration curve was obtained for the relationship between the 3/8-inch continuous-recording heat-transfer-probe indication and the 3-inch-diameter flat-face heat-transfer-rate model for a wide range of air-flow rates. Initial heat-transfer distributions were obtained at each air-flow condition by utilizing the thermocouples located around the 3-inch-diameter model. These tests were repeated at atmospheric pressure.

The heat-transfer rates were calculated on the Inconel heat-transfer models at the thermocouple locations by using the measured temperature rise rate of the back surface of the material. The heat-transfer-rate equation is

$$\dot{q} = \rho C_p \tau \frac{dT}{dt}$$

The dT/dt term can be obtained by recording temperature with time and the remaining quantities are a function of the type of material and location on the model surface.

Ablation Tests

The ablation specimens were measured and weighed before testing. The diameter and thickness were measured to the nearest one-thousandth of an inch and the weight was determined to the nearest one-thousandth of a pound.

The arc tunnel was started and brought up to the desired air-flow rate. The test specimen was inserted into the test section at a predetermined time by an automatic sequencer and removed from the stream after a specified time. Test duration for all materials was approximately 60 seconds. The free-stream pressure, free-stream temperature, air-flow rate, and heat-transfer rate (to 3/8-inch-diameter probe) were recorded continuously. The heat-transfer rate at the stagnation point on the 3-inch-diameter ablation specimen was determined from the calibration of the 3/8-inch probe. A motion-picture camera operating at 48 frames per second recorded the specimen appearance throughout the test. The specimens were measured and weighed again after the test.

The ablation calculations are discussed in the appendix.

TEST RESULTS AND DISCUSSION

Arc Unit Characteristics

The variation of the arc voltage, current, and total power with tunnel air-flow rate is shown in figure 7. The arc voltage increases approximately linearly with increased air-flow rate and the arc current decreased linearly with increased air-flow rate such that the total power remained approximately constant. Figure 8 shows that the arc voltage, current, and power are approximately constant with time.

Tunnel Calibration

A tabulation of the flow conditions and stagnation-point heat-transfer rate obtained on 3-inch-diameter flat-face heat-transfer model is given in table I. Figure 9(a) shows the variation of the free-stream pressure, free-stream temperature, and stagnation-point heat transfer on the 3-inch-diameter flat-face model with tunnel air-flow rate by using the air ejector and figure 9(b) shows the same quantities at a free-stream pressure of 1 atmosphere. The characteristics of the arc tunnel are such that at pressures below atmospheric the temperature of the stream is independent of the tunnel air-flow rate between 0.08 and 0.14 pound per second. At an air-flow rate above 0.14 pound per second, the free-stream temperature decreased with increased flow rate. It was observed during tunnel starting that the temperature increased with increased flow rate up to 0.08 pound per second. However, at atmospheric pressure the free-stream temperature appears to be independent of the tunnel air-flow rate over a range 0.08 to 0.22 pound per second.

A grid of the stagnation pressure and temperature at the stagnation point of a body in flight as a function of flight velocity and altitude is shown in

figure 10. Since in a low subsonic flow, the stagnation and free-stream pressures and temperatures approximately are equal, the shaded area in figure 10 indicates the stagnation pressures and temperatures that can be produced in the 6-inch subsonic arc tunnel.

In figure 9(a) it can be seen that for a given power setting a specific pressure (below atmosphere) and temperature in the test section dictates a definite tunnel flow rate. Thus, the only remaining parameter that can be used to duplicate the stagnation-point heat-transfer rate for a particular vehicle at a specific altitude and velocity is the model scale. At atmospheric pressure, the heat-transfer rate can be adjusted by varying the tunnel air-flow rate and model scale since the temperature is approximately constant over the air-flow-rate range covered in this report.

The heat-transfer distribution on the 3-inch-diameter flat-face cylinder as a function of distance from the stagnation point is shown in figure 11 at a tunnel-air-flow rate of 0.08 and a Mach number of approximately 0.14. The solid curve in figure 11 is a theoretical heat-transfer distribution for the same type of body (corner to body radius 0.090) from reference 6 at a Mach number of 6.0. The subsonic distribution has the same general shape up to the corner, $x/R = 1$. However, the heating above $x/R = 1$ is on the order of 50 percent of the stagnation point in the high-temperature subsonic stream. In a $M = 6$ stream, the heat transfer on the aft portion of the cylinder ($x/R > 1$) is on the order of 15 percent of the stagnation value. This approximate agreement of the heat-transfer distribution on the front surface is probably a characteristic of the facility and the model blocking effect in the subsonic stream. The heat-transfer distribution of the 3-inch-diameter flat-face cylinder varied only slightly on the aft portion with increased flow rate.

Ablation Results

A typical plot of operating conditions against time for the 6-inch subsonic arc tunnel is shown in figure 12. The heat-transfer rate was measured on the 3/8-inch-diameter probe and corrected to the cold-wall stagnation-point heat-transfer rate on the 3-inch-diameter flat-face cylinder.

The results of the ablation tests performed in the 6-inch subsonic arc tunnel are summarized in table II. The free-stream pressure, free-stream temperature, and cold-wall stagnation-point heat-transfer rates shown in table II are the average values recorded during specimen exposure. Since the test stream is low subsonic, $M \approx 0.15$, the stagnation temperature and pressure are approximately equal to the free-stream temperature and pressure. Therefore, the average stagnation enthalpy was determined from reference 4 by using the average free-stream pressures and temperatures. The wall enthalpy for Teflon was determined from the information in reference 7 by using an average ablation material mass-loss rate. The wall enthalpy for nylon was obtained from reference 8. The wall enthalpy for Teflon was used for Fluorogreen because the material is a Teflon product containing silica additives. The length change was determined from measurements of the specimen thickness at the stagnation point before and after testing. The effective heat of ablation was computed (from eq. (A5)).

The effective heat of ablation h_{eff} for Teflon, nylon, and Fluorogreen specimens are plotted against the boundary-layer enthalpy potential in figures 13, 14, and 15, respectively. In each case a straight line has been faired through the test points, and a linear extrapolation has been made to the ordinate line of zero boundary-layer enthalpy. The value of this ordinate H is called herein the zero enthalpy intercept.

For Teflon (fig. 13) the straight line defined by the test points may be represented by the equation:

$$h_{eff} = 500 + 0.433(h_s - h_w)$$

Also shown in figure 13 are theoretical and experimental curves from reference 9. The theoretical curve is represented by the equation:

$$h_{eff} = 950 + 0.46(h_s - h_w)$$

The experimental curve, obtained from data in a supersonic arc jet with heat-transfer rates from 250 to 860 Btu/ft^2-sec on one-half-inch-diameter models, is represented by the equation:

$$h_{eff} = 750 + 0.44(h_s - h_w)$$

The data obtained from the 6-inch subsonic arc tunnel reported herein yield an empirical curve which has a slope approximately equal to that reported in reference 7. There is, however, greater disparity in the value of H, the zero enthalpy intercept.

For nylon (fig. 14) the test points define a straight line represented by the equation:

$$h_{eff} = 400 + 0.605(h_s - h_w)$$

A comparison with another experimental curve from reference 8 that was obtained in a Mach 2 arc jet with heat-transfer rates of approximately 2,500 Btu/ft^2-sec on one-quarter-inch-diameter models can be seen in figure 14. The value of H was calculated for nylon (eq. (A7)) in reference 8 and the experimental points were used to determine the slope. The equation for nylon from reference 8 is:

$$h_{eff} = 550 + 0.56(h_s - h_w)$$

It can be seen in figure 14 that the agreement is very good in the range of enthalpy that can be obtained in this facility.

There is no available comparison for the Fluorogreen material at the present time. The empirical equation was found to be

$$h_{eff} = 100 + 0.54\left(h_s - h_w\right)$$

The intercept H was much less than anticipated because it was expected that, since the Fluorogreen is a combination of Teflon and a silica-based additive, the value of H would be more in the range of the Teflon value or higher. It was observed from the motion pictures that the silica additive formed droplets on the surface as the material ablated. The silica droplets were blown from the surface and never vaporized. Therefore, it can be assumed that the ablation temperature was above the melting point of the silica additive but less than the vaporization temperature. The ablation temperature of Teflon (1760° R) was used for the calculations that are presented in figure 15. The slope is approximately 25 percent greater than that for the pure Teflon.

CONCLUDING REMARKS

A 6-inch subsonic arc tunnel utilizing three-phase a-c water-cooled copper electrodes has been developed at the Langley Research Center to evaluate the performance of ablation materials under simulated reentry conditions. The tunnel is capable of producing a range of stagnation pressures from 0.16 to 1.0 atmosphere and stagnation temperatures up to 4400° K for periods of time up to 90 seconds limited by air storage capacity. Heat-transfer rates up to 70 Btu/ft^2-sec can be obtained on a 3-inch-diameter flat-face body in the 6-inch-diameter stream. Ablation materials can be evaluated in the stream at stagnation enthalpies up to 4,000 Btu/lb. Three commercially available materials, Teflon, nylon, and Fluorogreen, were tested as ablation materials in the 6-inch subsonic arc tunnel, and the results are in reasonable agreement with theoretical predictions and previously published experimental data.

Langley Research Center,
National Aeronautics and Space Administration,
Langley Station, Hampton, Va., January 7, 1963.

APPENDIX A

ABLATION CALCULATIONS

A theoretical development of ablation cooling equations can be found in references 10, 11, 12, and 13. The effective heat of ablation, the quantity of heat that can be absorbed by a unit mass of material, can be calculated from the relationship given in these references.

$$h_{eff} = \frac{\dot{q}_o}{\dot{m}} \tag{A1}$$

where $\dot{q}_o$ is the hot-wall heat-transfer rate and $\dot{m}$ is the mass loss per unit time per unit area. The heat-transfer rate is defined as

$$\dot{q}_o = \dot{q}_{s,i} \frac{h_s - h_w}{h_s - h_i} \tag{A2}$$

where $\dot{q}_{s,i}$ is the cold-wall heat-transfer rate. The mass loss per unit time per unit area for a subliming material can be calculated from the following equation:

$$\dot{m} = \rho \frac{dl}{dt} \tag{A3}$$

where ρ is the density and dl/dt is the change in length per unit time. It was necessary to make the approximation that

$$\frac{dl}{dt} = \frac{l_f - l_i}{t_f - t_i} = \frac{\Delta l}{\Delta t} \tag{A4}$$

because measurements could be obtained only before and after each test. Therefore, the effective heat of ablation for this type of measurement can be expressed as

$$h_{eff} = q_{s,i} \frac{h_s - h_w}{h_s - h_i} \frac{\Delta t}{\rho \, \Delta l} \tag{A5}$$

The effective heat of ablation is also given in the above references as follows:

$$h_{eff} = H + K(h_s - h_w) \tag{A6}$$

where

$$H = C_{p,b}\left(T_w - T_b\right) + h_v + h_m \tag{A7}$$

and

$$K = \frac{C_{p,2}}{C_{p,1}}\left(1 - \frac{1}{3N_{PR}^{0.6}}\right) \tag{A8}$$

When the effective heat of ablation calculated from equation (A5) is plotted against the enthalpy difference across the boundary layer, $\left(h_s - h_w\right)$, H is the intercept, and K is the slope of the curve. Thus, K can be evaluated experimentally.

$$K = \frac{h_{eff} - H}{h_s - h_w} \tag{A9}$$

REFERENCES

1. Hunczak, Henry R., and Rousso, Morris D.: Starting and Operating Limits of Two Supersonic Wind Tunnels Utilizing Auxiliary Air Injection Downstream of the Test Section. NACA TN 3262, 1954.

2. Howell, Robert R.: Experimental Operating Performance of a Single-Stage Annular Air Ejector. NASA TN D-23, 1959.

3. Pearce, Willard J.: Plasma Jet Temperature Study. WADC Tech. Rep. 59-346 (Contract No. AF 33(616)-5848), U.S. Air Force, Feb. 1960.

4. Moeckel, W. E., and Weston, Kenneth C.: Composition and Thermodynamic Properties of Air in Chemical Equilibrium. NACA TN 4265, 1958.

5. Gardon, Robert: An Instrument for the Direct Measurement of Intense Thermal Radiation. Rev. Sci. Instr., vol. 24, no. 5, May 1953, pp. 366-370.

6. Beckwith, Ivan E., and Cohen, Nathaniel B.: Application of Similar Solutions to Calculation of Laminar Heat Transfer on Bodies with Yaw and Large Pressure Gradient in High-Speed Flow. NASA TN D-625, 1961.

7. Steg, Leo: Materials for Re-Entry Heat Protection of Satellites. ARS Jour., vol. 30, no. 9, Sept. 1960, pp. 815-822.

8. Chapman, Andrew J.: An Experimental Investigation of Several Ablation Materials in an Electric-Arc-Heated Air Jet. NASA TN D-1520, 1963.

9. Georgiev, Steven, Hidalgo, Henry, Adams, Mac C.: On Ablation Recovery of Satellites. AVCO Res. Rep. 47 (Contract AF 04(647)-278), AVCO Res. Lab., Mar. 6, 1959.

10. Roberts, Leonard: Mass Transfer Cooling Near the Stagnation Point. NASA TR R-8, 1959. (Supersedes NACA TN 4391.)

11. Roberts, Leonard: A Theoretical Study of Stagnation-Point Ablation. NASA TR R-9, 1959. (Supersedes NACA TN 4392.)

12. Roberts, Leonard: Stagnation-Point Shielding by Melting and Vaporization. NASA TR R-10, 1959.

13. Roberts, Leonard: An Approximate Analysis of Unsteady Vaporization Near the Stagnation Point of Blunt Bodies. NASA TN D-41, 1959.

TABLE I.- 6-INCH SUBSONIC HIGH-TEMPERATURE ARC TUNNEL TEST CONDITIONS

ON 3-INCH-DIAMETER FLAT-FACE INCONEL MODEL

Tunnel air-flow rate, lb/sec	Free-stream temperature, ^{o}K	Free-stream pressure, atm	Cold-wall heat-transfer rate, Btu/ft^2-sec	Free-stream velocity, ft/sec	Mach number	Reynolds number/ft
0.083	4350	0.16	60.3	630	0.15	6,600
.138	4400	.26	73.6	650	.15	10,900
.218	3700	.40	64.4	540	.14	18,900
.084	3650	1.0	39.1	80	.02	7,400
.137	3750	1.0	49.2	135	.04	11,900
.214	3650	1.0	53.0	200	.05	19,500

TABLE II.- ABLATION MATERIAL TESTS

Material	Material density, lb/cu ft	Average free-stream pressure, atm	Average stagnation enthalpy, Btu/lb	Wall enthalpy, Btu/lb	Average cold-body heat-transfer rate, Btu/ft^2-sec	$\frac{\dot{q}_o}{\dot{q}_{s,i}}$	Test time, sec	Length change, in.	Effective heat of ablation, Btu/lb	Boundary-layer enthalpy potential, Btu/lb
Teflon*	137.5	0.40	3,070	440	64.6	0.892	60.3	0.192	1,620	2,630
Teflon	137.5	.16	3,950	440	65.2	.917	60.4	.154	2,060	3,510
Teflon	137.5	.26	3,770	440	66.0	.913	45.8	.124	1,845	3,330
Teflon	137.5	.16	4,140	440	67.0	.923	59.2	.151	2,130	3,700
Nylon**	70.7	.40	3,030	290	67.2	.942	59.9	.315	2,040	2,740
Nylon	70.7	.16	4,060	290	66.6	.959	60.2	.247	2,650	3,770
Nylon	70.7	.16	4,190	290	69.2	.959	59.9	.239	2,830	3,900
Fluorogreen	140.0	.40	3,160	440*	64.3	.890	59.9	.190	1,560	2,700
Fluorogreen	140.0	.16	3,930	440	63.5	.919	59.3	.150	2,000	3,490
Fluorogreen	140.0	.16	4,210	440	71.1	.923	60.3	.155	2,190	3,770

*Reference 7.
**Reference 8.

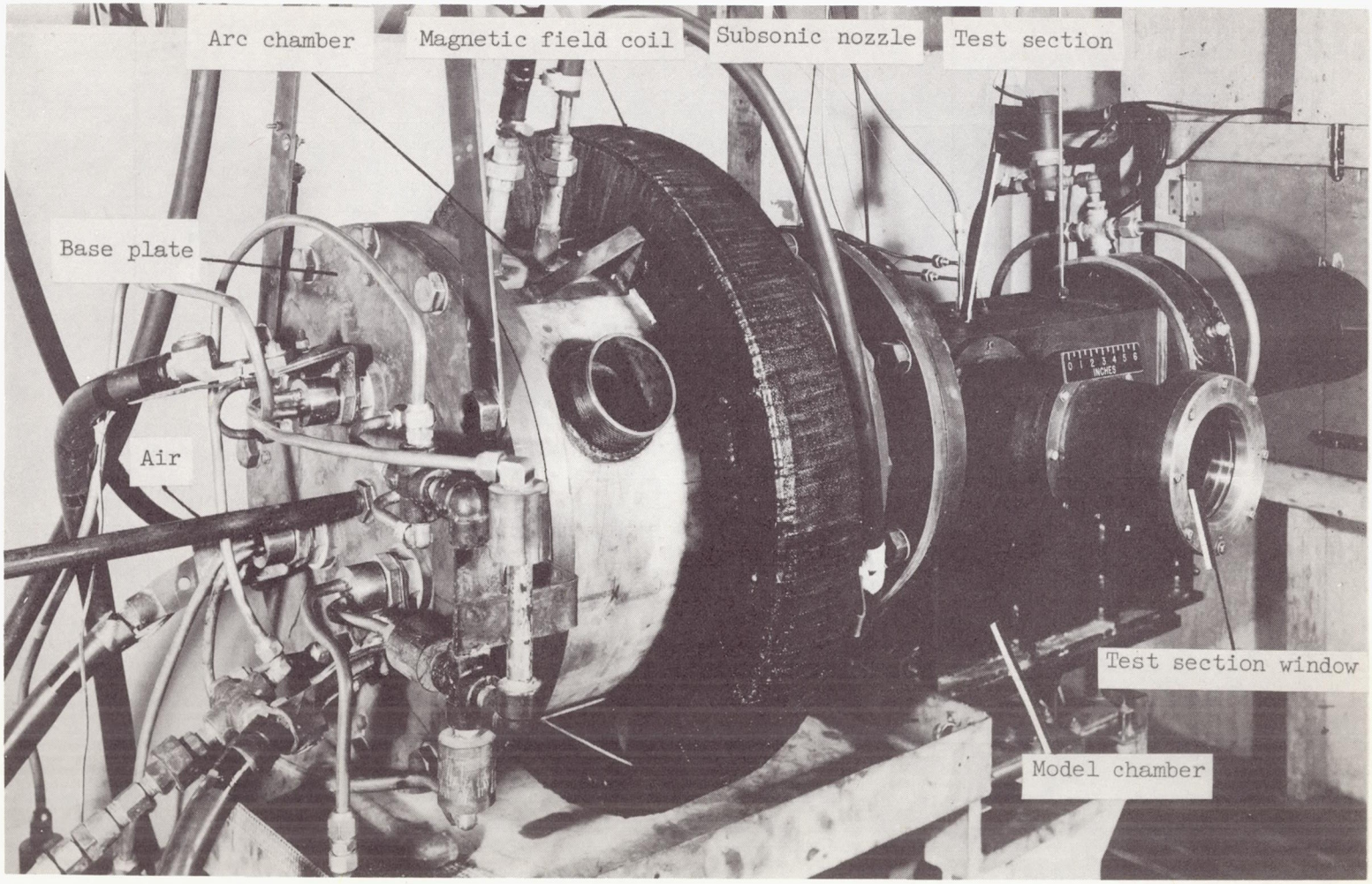

Figure 1.- Photograph of 6-inch subsonic arc tunnel. L-60-3831.1

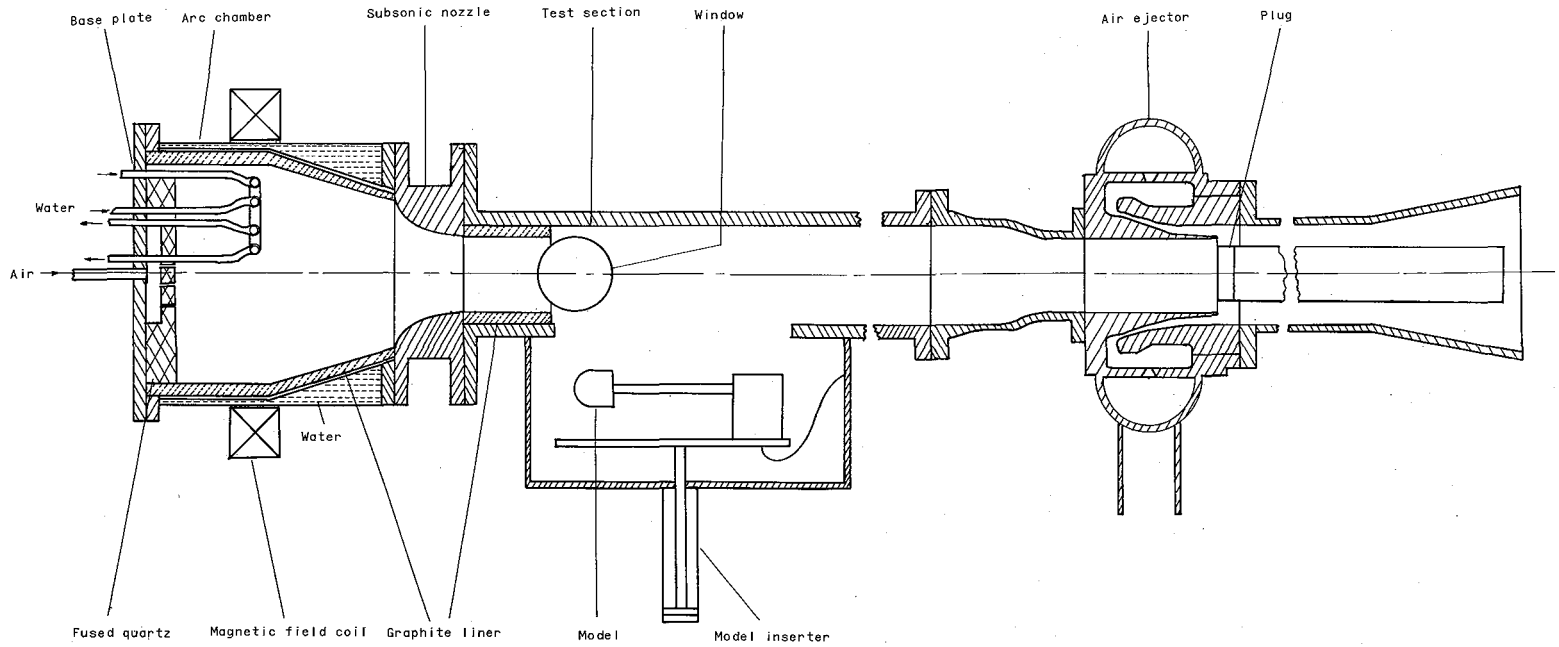

Figure 2.- Sketch of 6-inch subsonic arc tunnel.

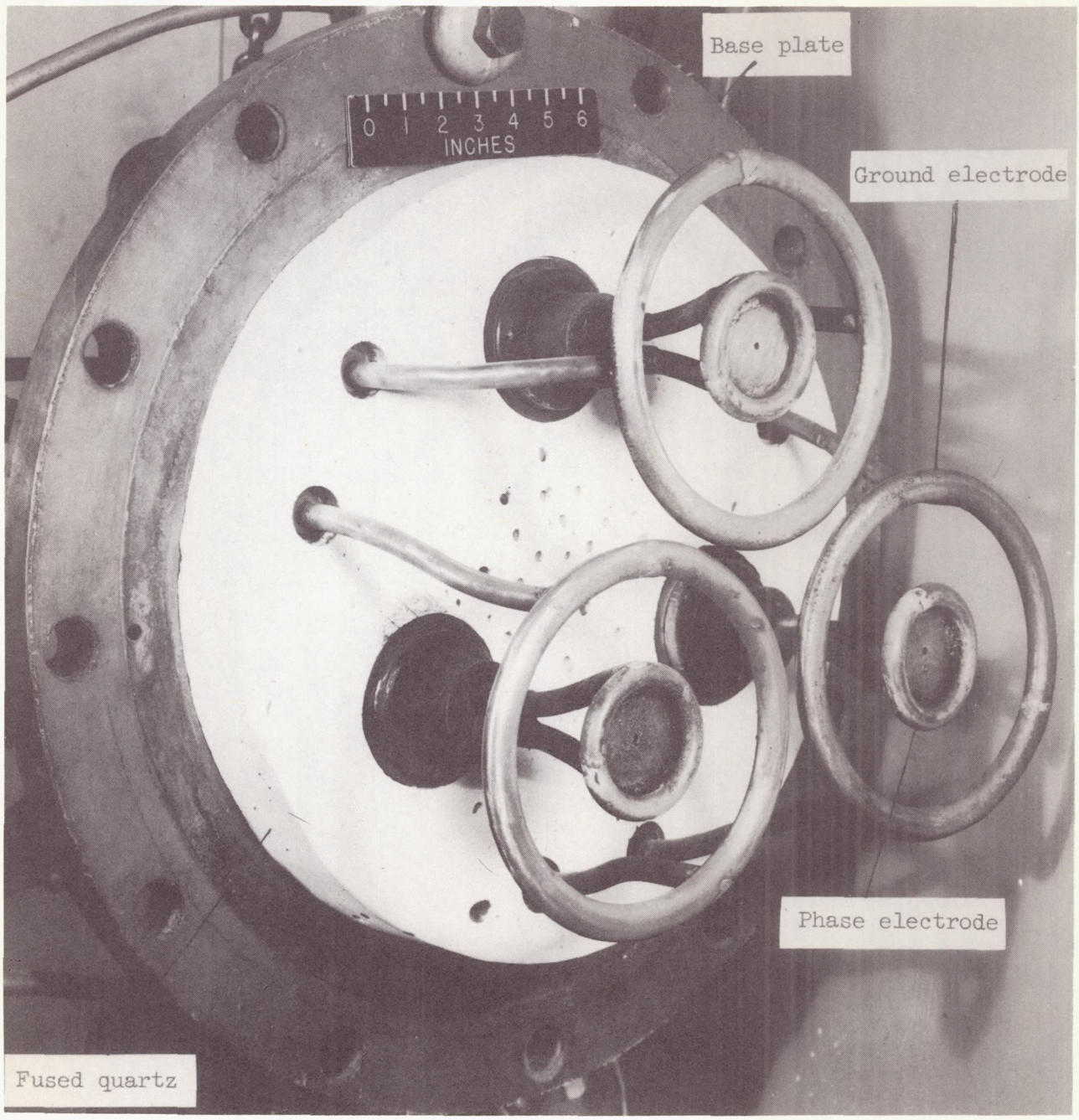

Figure 3.- Three-phase water-cooled copper-ring electrode configuration. L-60-3835.1

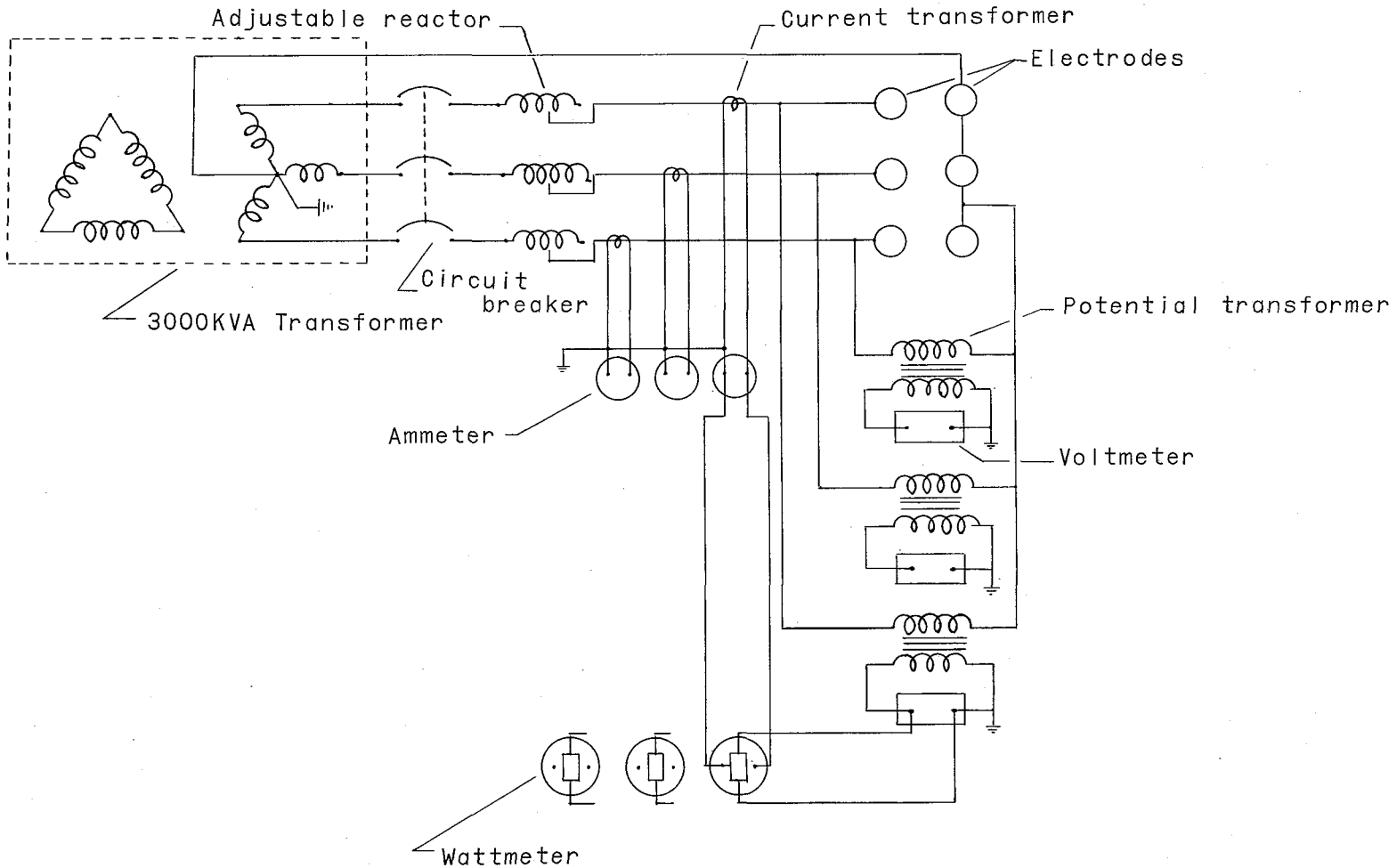

Figure 4.- Schematic diagram of power supply and measuring system.

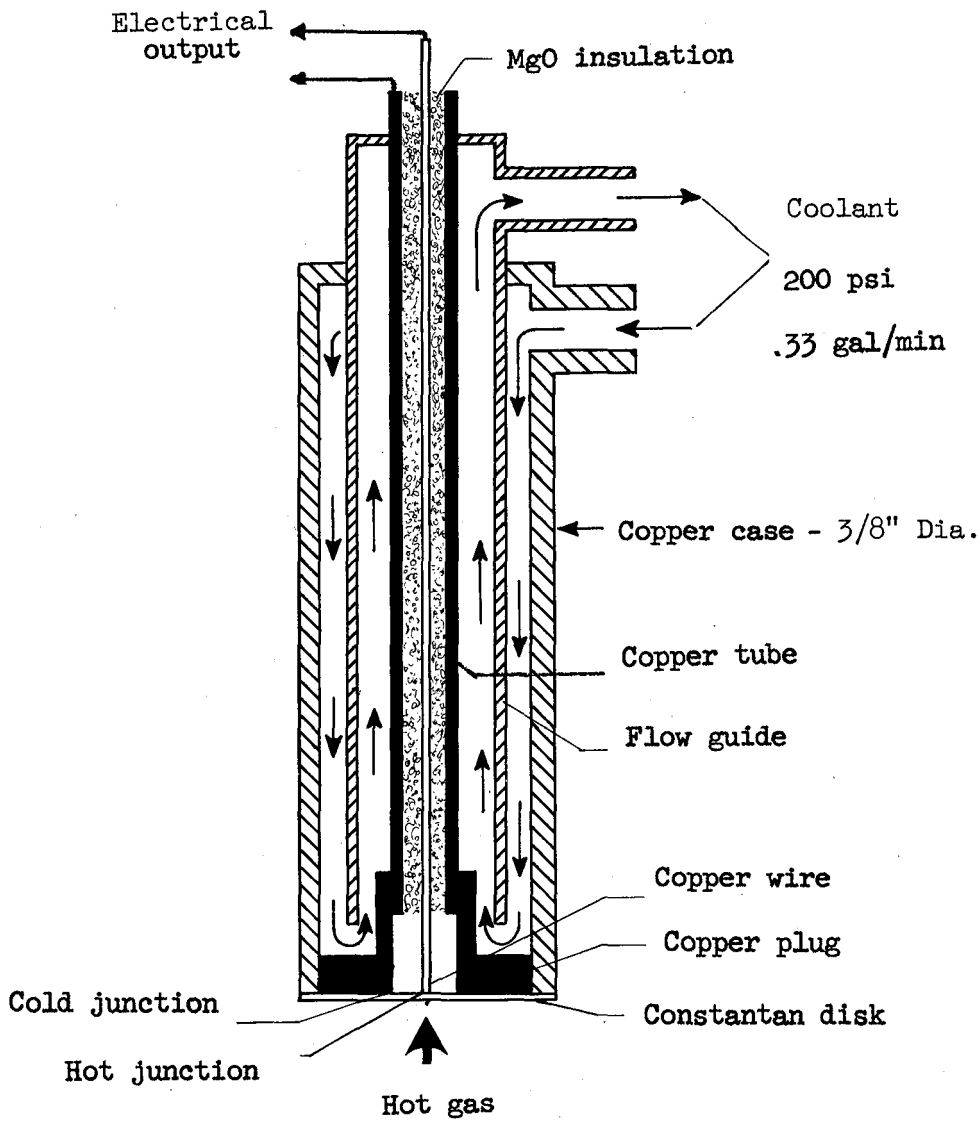

Figure 5.- Continuous recording heat-transfer-rate probe.

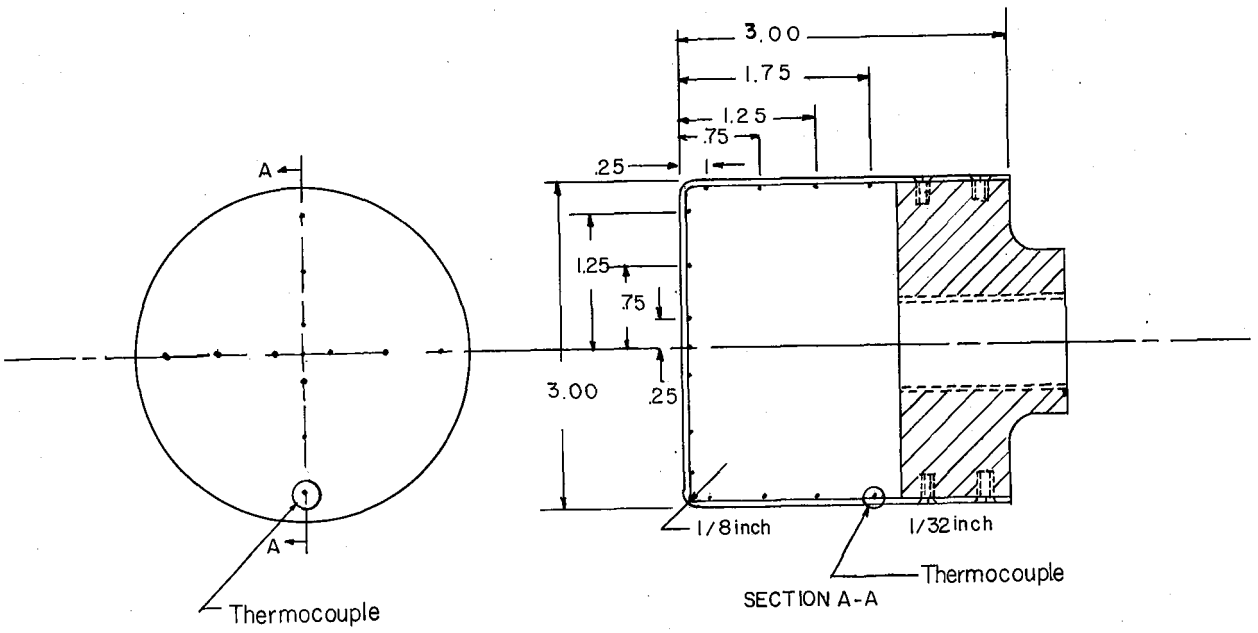

(a) Flat-face heat-transfer calorimeter.

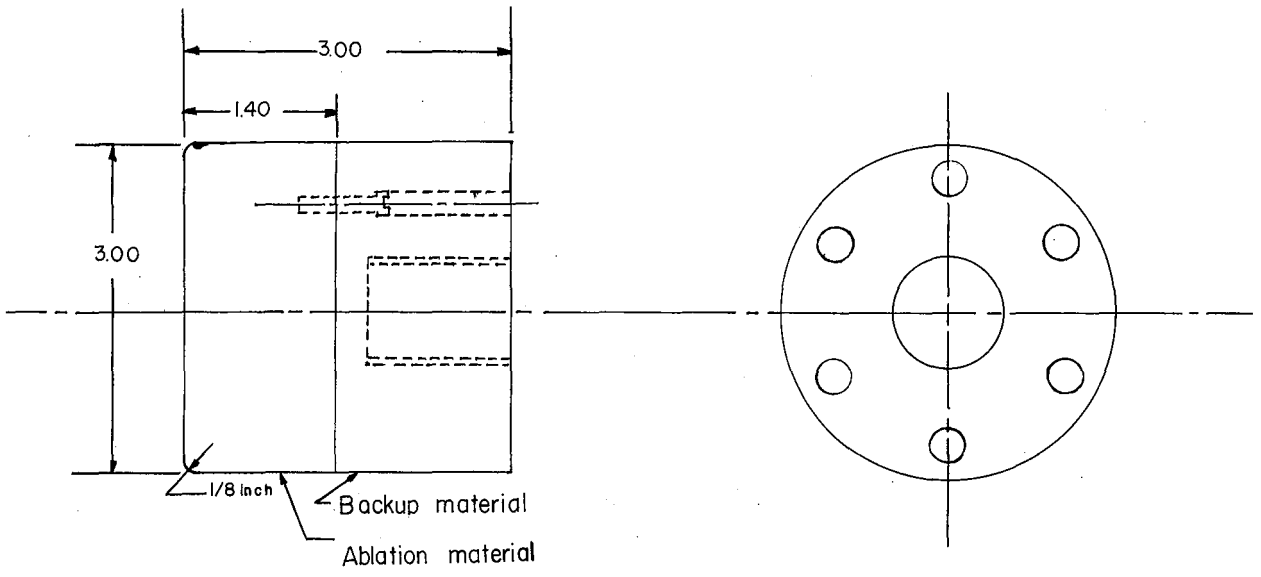

(b) Ablation model.

Figure 6.- Three-inch-diameter flat-face heat-transfer calorimeter and ablation model.

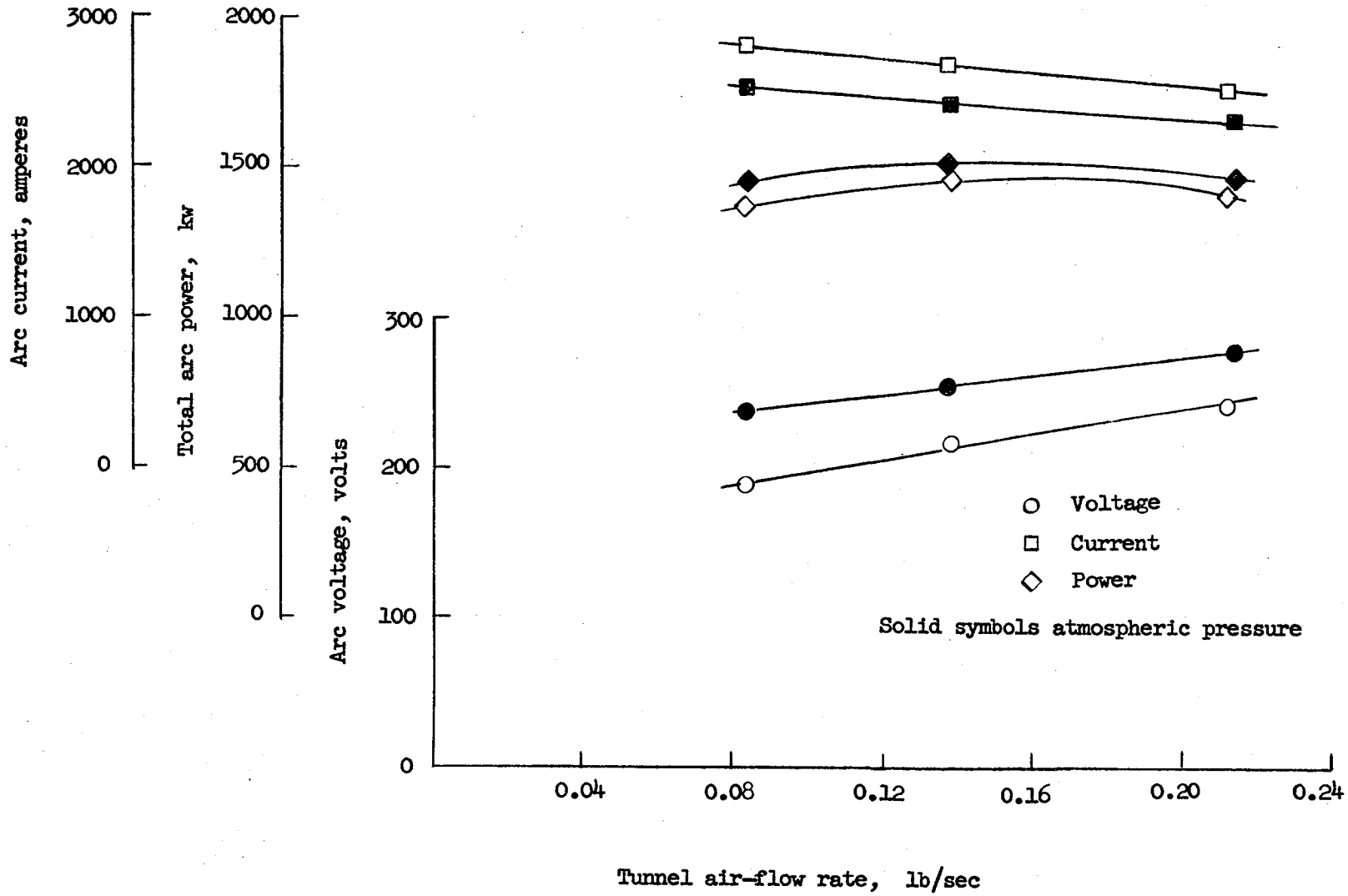

Figure 7.- Electrical characteristics of three-phase alternating-current arc unit.

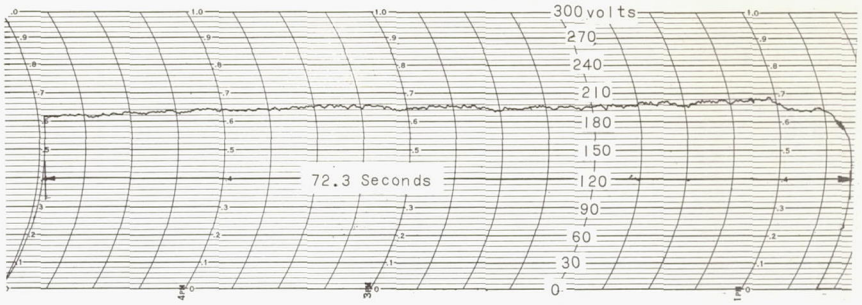

ARC VOLTAGE phase 2

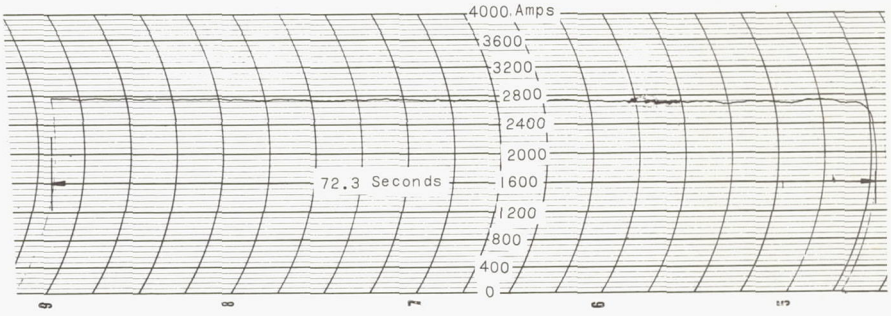

Arc current phase 2

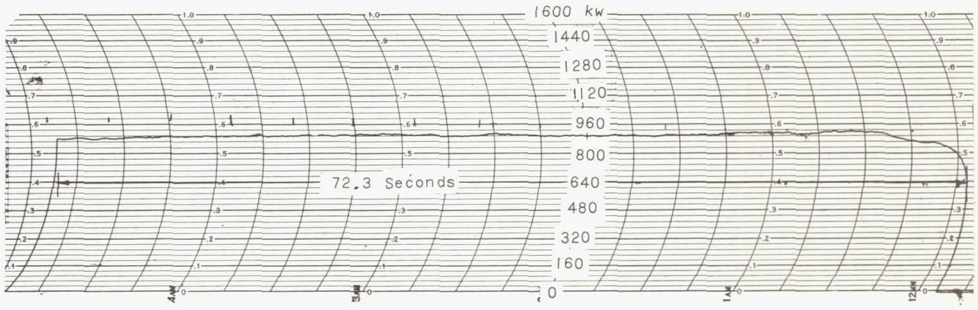

Arc power phases 1 and 2

Figure 8.- Arc voltage, current, and power as a function of time for the 6-inch subsonic arc tunnel.

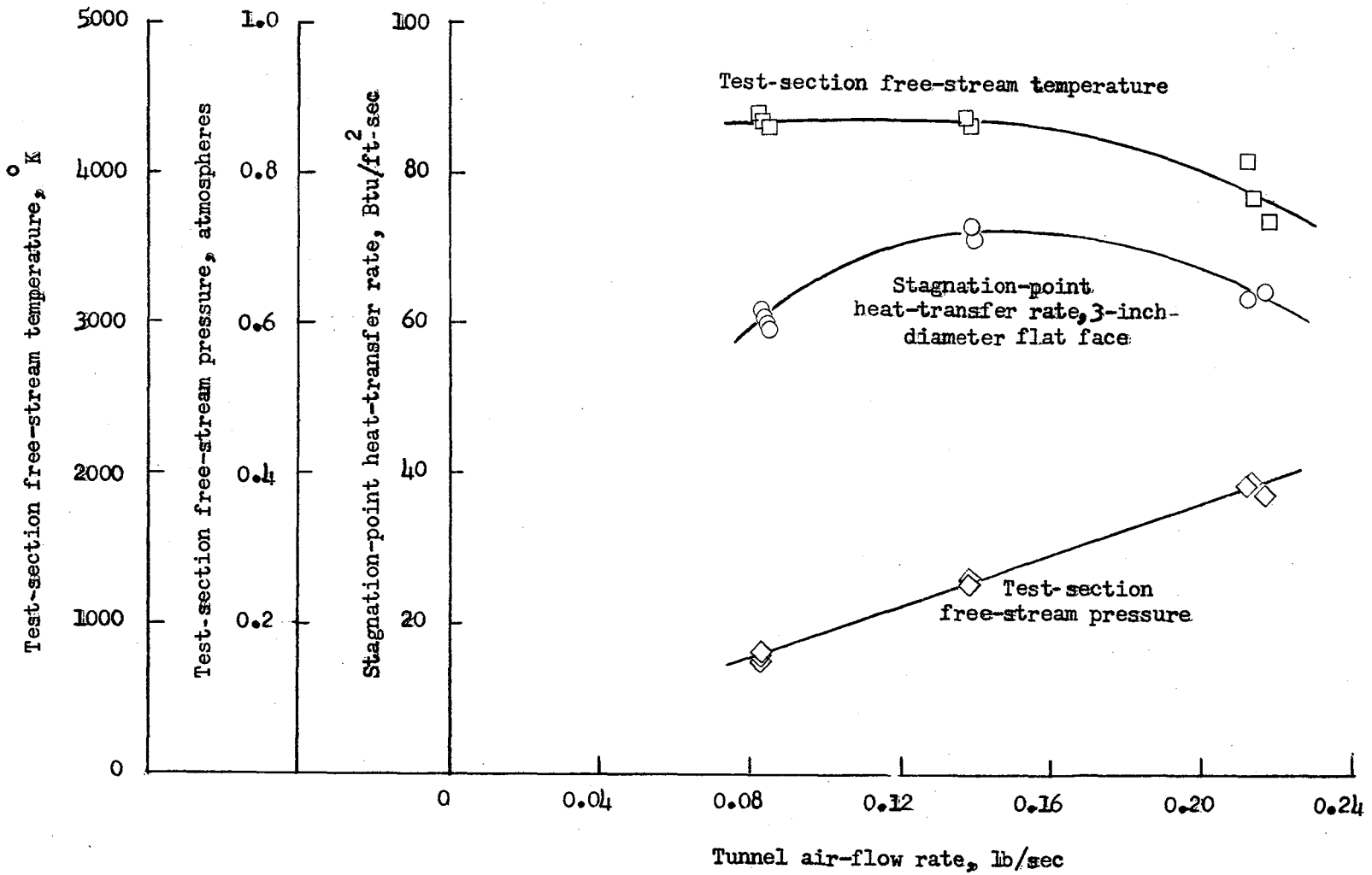

(a) 6-inch subsonic arc tunnel.

Figure 9.- Operating characteristics.

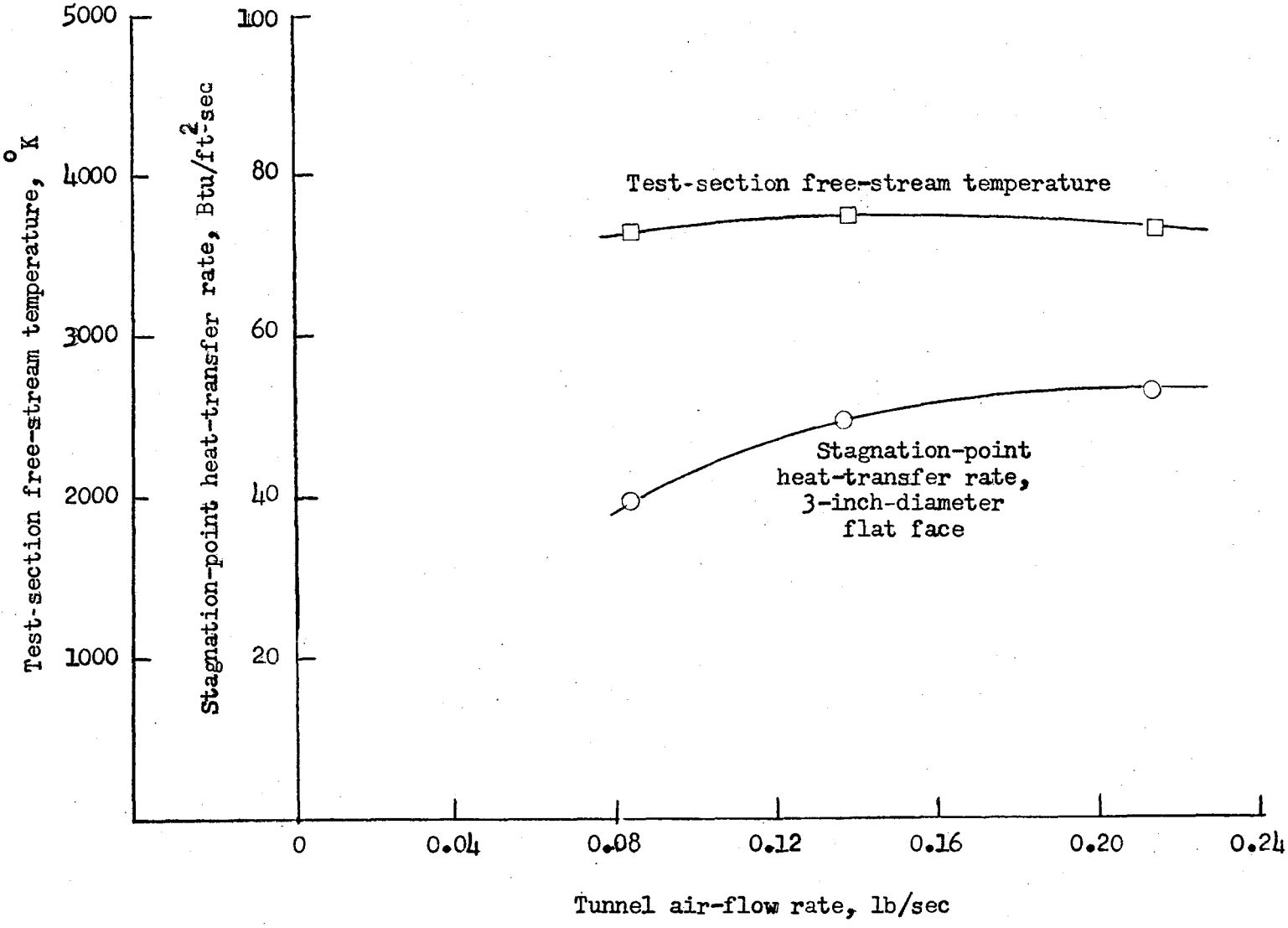

(b) 6-inch subsonic arc tunnel at atmospheric pressure.

Figure 9.- Concluded.

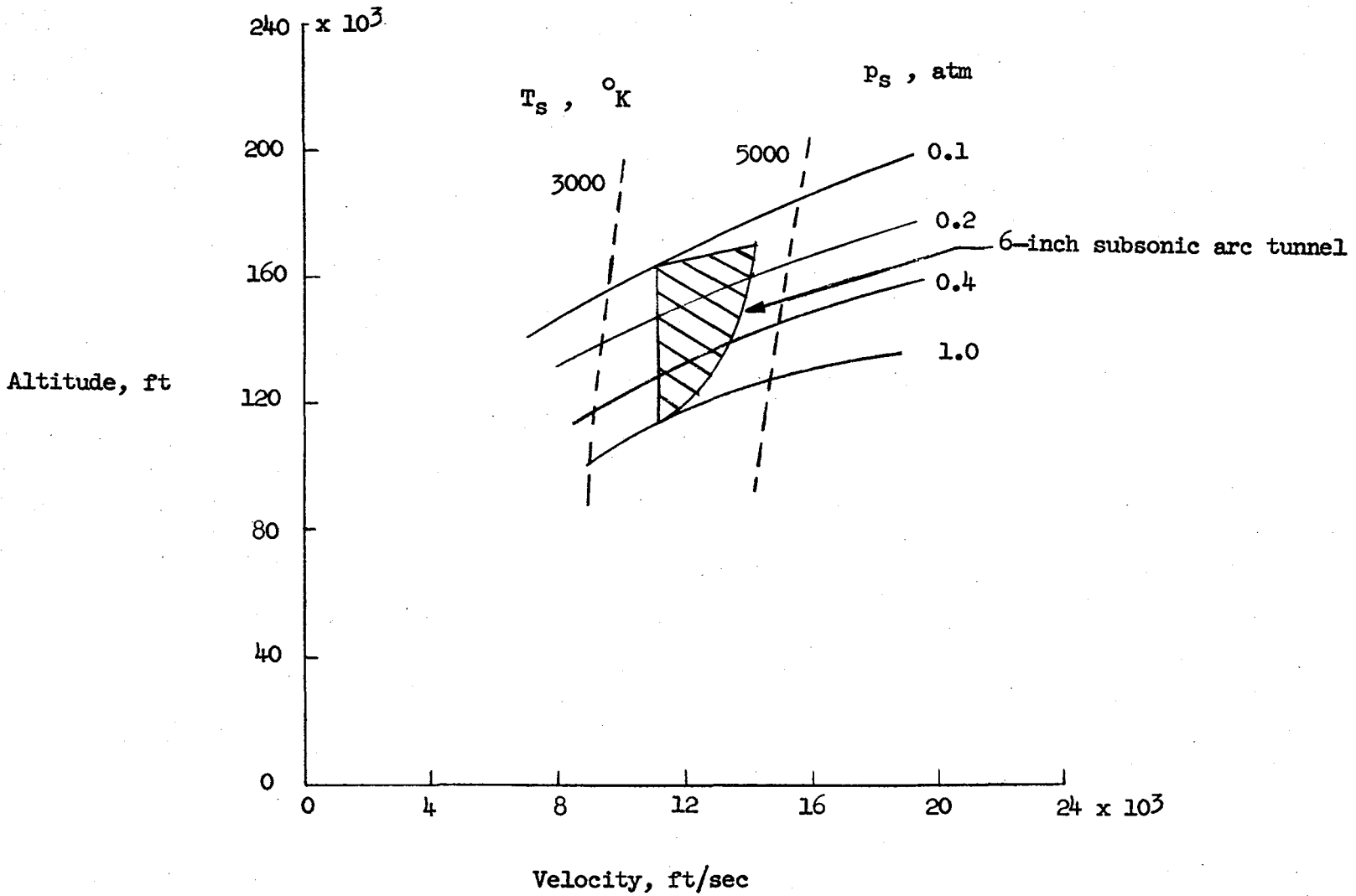

Figure 10.- Simulation capability of 6-inch subsonic arc tunnel.

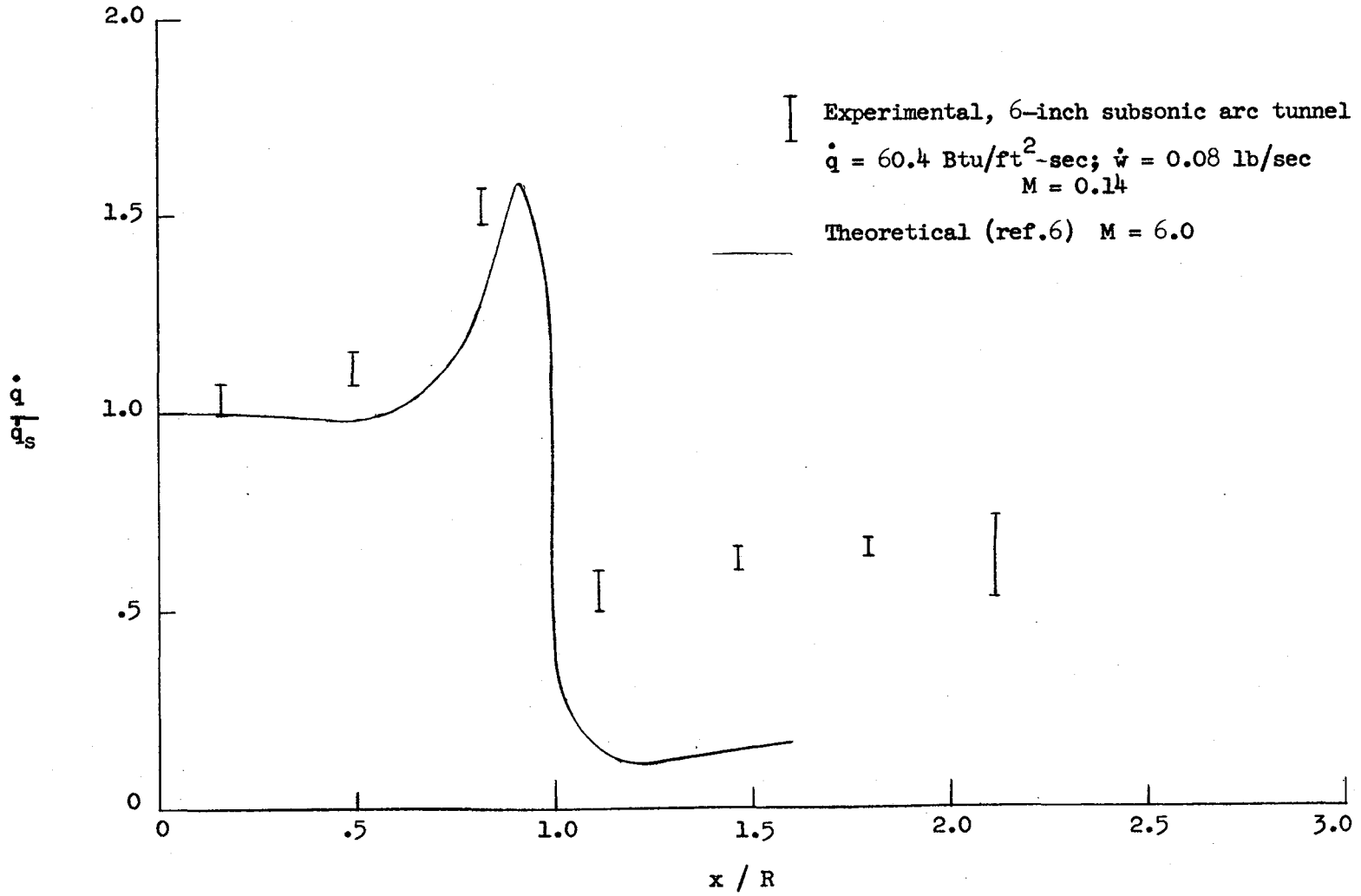

Figure 11.- Heat-transfer distribution on a 3-inch-diameter flat-face model.

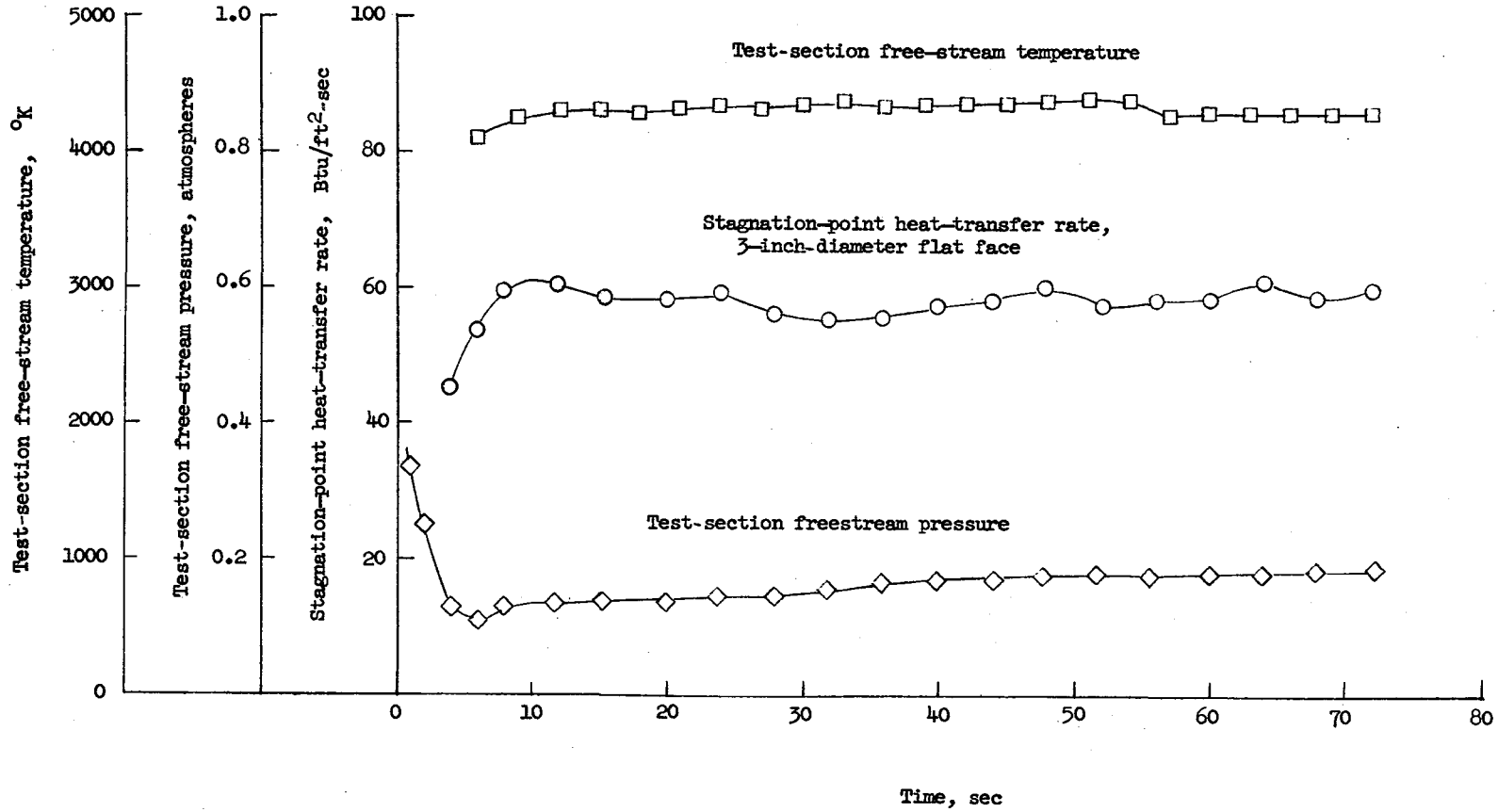

Figure 12.- Operating characteristics as a function of time for the 6-inch subsonic arc tunnel.

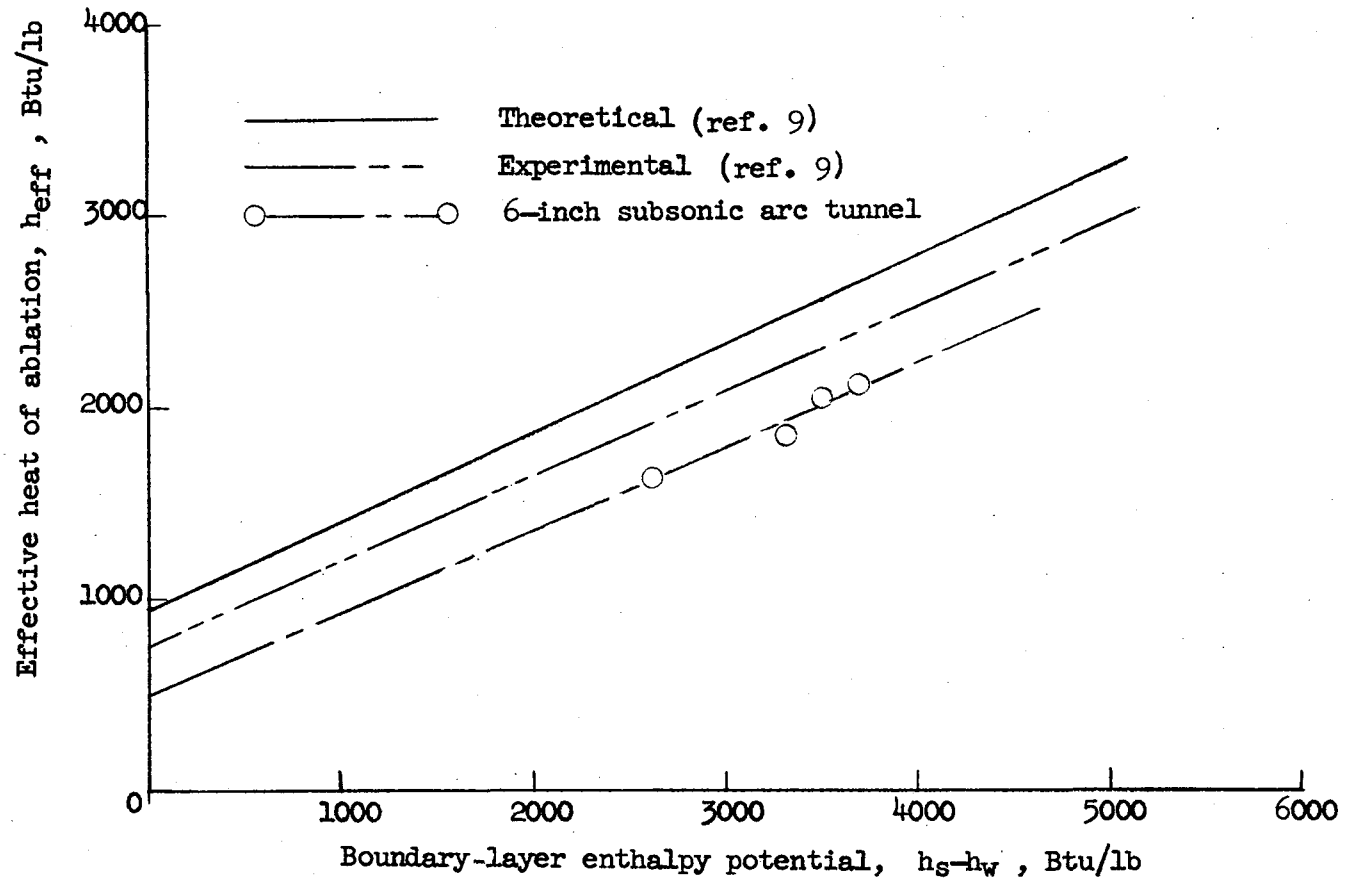

Figure 13.- Variation of effective heat of ablation with boundary-layer enthalpy potential for Teflon.

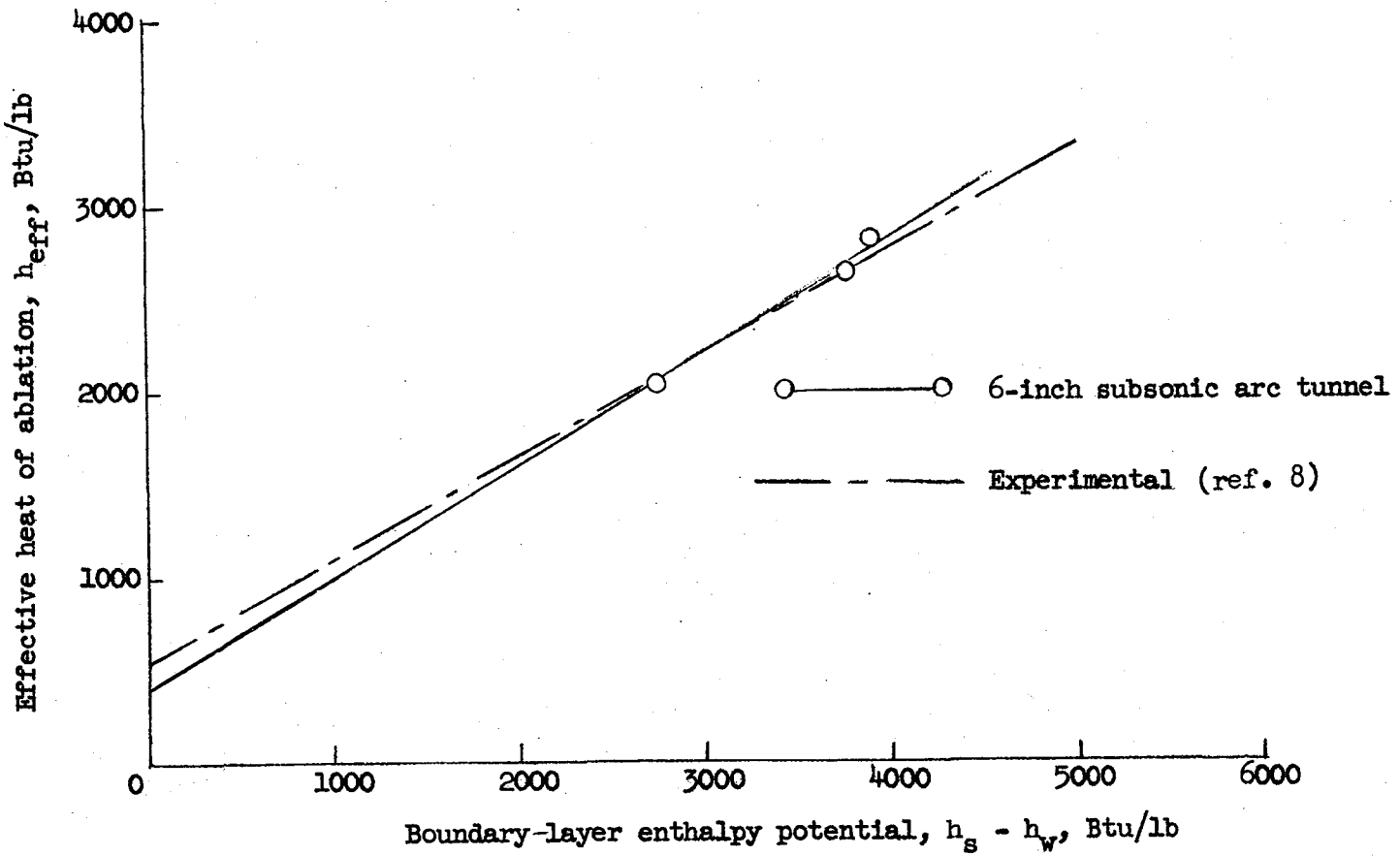

Figure 14.- Variation of effective heat of ablation with boundary-layer enthalpy potential for nylon.

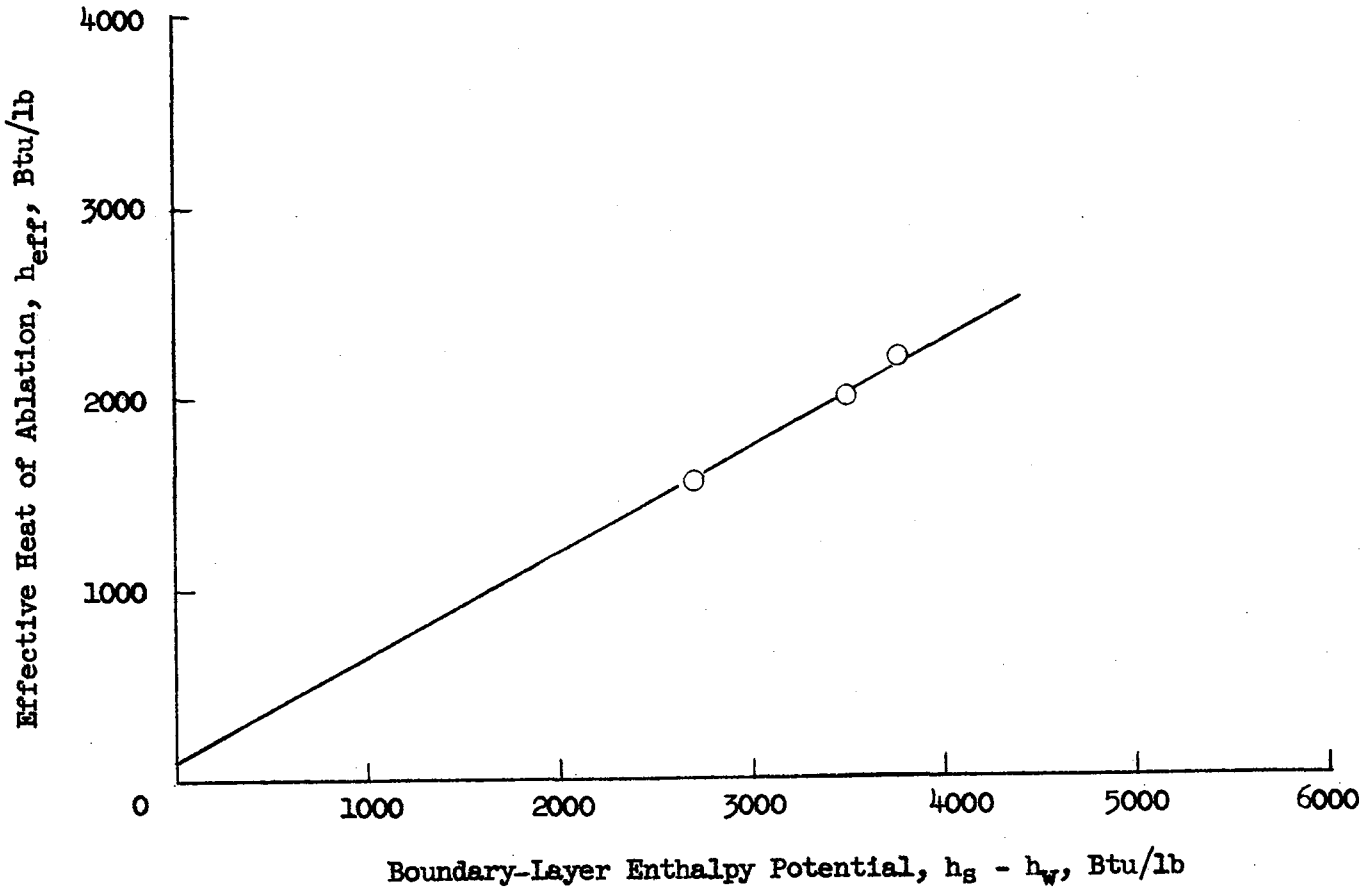

Figure 15.- Variation of effective heat of ablation with boundary-layer enthalpy potential for Fluorogreen.